

Damage and Defect Detection in Composites Using Millimetre Wave Permittivity Measurement

C. M. Alabaster, J. S. Dahele and R. A. Badcock, Cranfield University.

E-mail: c.m.alabaster@rmcs.cranfield.ac.uk

Abstract.

A free space measurement of permittivity within the millimetre wave band is employed to detect and locate defects within fibreglass composite samples. This technique offers a non-contacting and non-destructive method of locating a variety of defects. The millimetric wave experimental technique is described and its theoretical basis is supplied. Experiments have been conducted on twelve samples of composite materials some of which were nominally ideal control samples; others had damage induced within them deliberately. The defect categories were: low-level impact damage, incomplete cure and vacuum release during cure. Ultrasound C-scan imaging was used to confirm the presence/absence of defects in each sample. The permittivity of a large planar sample was mapped and found to be reasonably consistent. The measured permittivity data is then studied to determine the feasibility of identifying the defects. The results demonstrate the ability to resolve defects from nominally ideal material and to identify the nature of the defect. The experimental method can also detect low-level impact damage with a superior sensitivity to that of the ultra-sound imaging technique. The spatial resolution of the millimetric technique is around 40mm or better.

Keywords: composites, permittivity, millimetre wave, defect detection, damage detection.

I INTRODUCTION

Radio frequency (RF) measurements offer the potential to determine the structural integrity of composite materials in a non-destructive, non-contacting manner. Defects such as delaminations, voids, matrix cracks and improper cure result in changes in the dielectric properties of the composite ^[1]. The presence of such defects may be determined via a measurement of dielectric properties, such as permittivity, or by the absorption, scattering and reflections of an electromagnetic (EM) signal, propagating in the medium, which is incident on a discontinuity resulting from the defect. Ideally, one would desire a diagnostic tool which is non-contacting and capable of achieving a spatial resolution in the order of the likely defect dimensions. The non-contacting requirement dictates a free-space RF based measurement and the requirement for fine resolution dictates the use of millimetre wave (MMW) frequencies (30GHz to 300GHz). The use of MMW in this role was discussed by Gopalsami, Bakhtiari et al ^{[1][2]} in which a 75 to 110GHz imaging system was developed and employed to detect sub-surface voids and disbonds in Kevlar/epoxy composite samples. Millimetric measurements also offer a high contrast between defective and nominally ideal material.

This paper describes some experimental work to determine the feasibility of a free-space measurement of permittivity in the 90GHz to 100GHz band to detect and locate a variety of defects in planar fibreglass composite samples. Several composite samples were manufactured; some being kept as control samples having no defects and others having damage induced within them. The defect categories were: low-level impact damage, incomplete curing and vacuum release during the curing cycle. Additionally, a large sheet of composite sample was manufactured and the spatial variation in its permittivity was mapped. This sample was subsequently subjected to a low-level impact damage and then re-examined using the MMW technique in order to judge the spatial resolution to which the defect can be resolved. The structural integrity of all composite samples has been determined using a Physical Acoustics UltraPAC II ultra-sound imaging C-scan with a 5 MHz probe to enable a comparison between the MMW measurements and the severity and extent of defects.

Section (II) describes the theory which underpins the measurement method. In section (III) the experimental set up and calibration method are described and details are given of the method of processing the measured data in order to determine the sample permittivity. This section also describes the sample preparation, defects and ultra-sound testing. The results of the MMW permittivity measurements and ultra-sound images are given in section (IV). Finally, section (V) draws some conclusions, chief amongst which are that there are resolvable differences in the permittivity between nominally ideal and defective samples.

II THEORY^{[3][4]}

A plane wave normally incident on a slab of dielectric sample of thickness t_s is partially reflected, transmitted and absorbed by the dielectric. The reflected and transmitted signals are comprised of an infinite number of components due to the multiple reflections between the air/dielectric interfaces. Thus the total reflected and transmitted signals are given respectively by:

$$r = \frac{r_1 - r_1 \exp(-2k_s t_s)}{1 - r_1^2 \exp(-2k_s t_s)} \quad (1)$$

and

$$t = \frac{(1 - r_1^2) \exp(-k_s t_s)}{1 - r_1^2 \exp(-2k_s t_s)} \quad (2)$$

where k_s is the propagation constant in the sample and r_1 is the reflection coefficient of the sample/air interface. Both are functions of the relative complex permittivity, ϵ_r , of the sample given by:

$$r_1 = -\frac{\sqrt{\epsilon_r} - \sqrt{\epsilon_0}}{\sqrt{\epsilon_r} + \sqrt{\epsilon_0}} \quad (3)$$

and

$$k_s = k_0 \sqrt{\epsilon_r} \quad (4)$$

where k_0 and ϵ_0 are the propagation constant and permittivity in free space, respectively.

The measured values of the reflection and transmission coefficients are R_m and T_m respectively and relate to r and t by the equation pair:

$$R_m = 20 \log_{10} |r| \quad dB \quad (5a)$$

and

$$T_m = 20 \log_{10} |t| \quad dB \quad (5b)$$

Wideband solutions of R_m and T_m indicate cyclical variations with frequency due to the multiple reflections between interfaces beating in and out of phase. The frequencies of peaks and troughs occur when the sample thickness is a multiple of a quarter wavelength and may be used to provide an initial estimate of ϵ_r . Note that permittivity (and hence relative permittivity) is a complex quantity i.e. $\epsilon_r = \epsilon_r' - j\epsilon_r''$, where ϵ_r' is the relative dielectric constant and ϵ_r'' is the relative loss factor.

III EXPERIMENTAL Work

A Experimental Set Up

A method similar to that of Ma and Okamura^[5] was employed and has also been described in previous publications^{[3] [4]}. Circular samples were clamped on to an annular sample frame placed mid-way between a pair of standard gain waveguide horns connected to a vector network analyser (VNA). T_m and R_m were measured via the VNA $|S_{21}|$ and $|S_{11}|$ paths, respectively, over the frequency band 90 to 100GHz. This method requires that only the amplitudes of the transmission and reflection coefficients need be measured and that there is no need for phase data. The amplitudes only method reduces the requirement to accurately

maintain the positional and alignment accuracy of the equipment and to maintain the phase and frequency stability of the VNA source. The chosen frequency band represents a compromise between spatial resolution, which improves as frequency increases, and the availability of test equipment and components which accompanies technological developments to exploit the atmospheric window at 94GHz. Furthermore, the band is restricted to 10GHz since it is assumed in the processing of measured data that the samples exhibit a negligible degree of dispersion.

The horns were aligned for vertical polarisation, parallel with each other and for normal incidence on the sample. Lähteenmäki and Karttaavi ^[6] have concluded that misalignment errors of up to 3° have minimal effects on the results. Furthermore, the authors own experience suggests that T_m and R_m are relatively insensitive to small alignment errors. The sample was positioned just beyond the far field threshold of each horn ($= 2D^2/\lambda$, where D = the horn aperture and λ = the longest wavelength) to ensure plane wave incidence. Measurements at 90 to 100GHz required a horn to sample separation of 110mm. The samples were disc shaped of diameter 125mm but with a region exposed to the MMW of 105mm in diameter; the 10mm around the periphery enabling each sample to be clamped to the annular sample frame. The -3dB contour of the beam in the sample plane approximates to a circle of diameter 40mm. Samples were therefore sufficiently large to subtend an angle of greater than twice the -3dB beamwidth of the horns; thus they intercepted the entire main beam (at least the first 15 Fresnel zones) and approximate to an infinitely large sample.

B Calibration

The VNA was operated in a time gated mode in order to isolate the first reflection from the sample (reflection measurement) and the main through path between horns (transmission measurement). In this way multiple reflections between the horns and/or sample are ignored and do not corrupt the reading. The reflection measurement was calibrated with respect to a metal plate fitted in place of the sample. All reflection coefficients were therefore normalised

to that of a short circuit in the measurement plane. The transmission measurement was calibrated with respect to the path loss with no sample in place.

C Data Processing

In the general case, equations (1) to (5) are solved using an iterative technique to find solution(s) for ϵ_r . Solutions for ϵ_r are sought over a user defined search space and resolution which result in computed values of transmission and reflection coefficients which most closely match the measured values T_m and R_m . However, due to the multiple reflections present in all but very lossy samples, multiple solutions of ϵ_r may be found. This ambiguity can easily be overcome based on an initial estimate from the peak and trough frequencies or by fitting data at several nearby frequencies. T_m and R_m were recorded every 2GHz over the band 90 to 100GHz and solutions for ϵ_r were computed for which the rms percentage error between computed and measured transmission and reflection coefficients at all six frequencies was a minimum. No solutions were declared in the cases where the rms percentage error exceeded 20%. This was an arbitrary threshold beyond which it was deemed that there was too great an inconsistency between measured and computed results.

D Samples

Twelve Fibreglass composite samples were manufactured from Fibredux 916G, a woven pre-preg tape (10 layers, all aligned). All but sample 12 were manufactured as a disc of diameter 125mm, sample 12 was a sheet of dimensions 500mm x 250mm. Table (i) summarises the details of the twelve samples. Three samples of each control and defect category (except impact damaged samples) were manufactured in order to judge the statistical spread of results.

All the samples were cut from the same sheet and all were processed in the same way prior to curing. The curing process was carried out under a vacuum of 200mbar. The woven pre-preg tape Fibredux 916G were cured by temperature ramping at a rate of 1.5°C per minute to

a final temperature of 130°C followed by a dwell at this temperature for 30 minutes. The samples were cooled down by opening the door after switching the oven off. The vacuum was released and the samples removed from the oven. The vacuum was released at 80°C for the samples that had the vacuum released early, otherwise the cure cycle continued as per normal. The incompletely cured samples were removed from the oven once it had reached its final temperature i.e. zero dwell time.

The quality of every sample was assessed using a 5MHz ultra-sound imaging C-scanner. The samples were supported in water above the bottom of the water tank and the transducer acquired an image of the sample in a raster scanning fashion. The ultra-sound equipment was operated in a time gated mode to capture the two-way transmission path of the signal (through the sample, reflected from the tank base and back through the sample). Undamaged composite material transmits the signal through it with little attenuation, whereas the presence of defects scatters and absorbs the signal resulting in a highly attenuated transmission path. A representative sample of the ultra-sound images is given in figure 1.

E Experimental Tests

Initial measurements were made on a sample of PTFE in order to validate the method since the permittivity of PTFE in the band 90 to 100GHz is reasonably well established.

The permittivity of samples 1 to 11 was measured at a consistent sample orientation. The impact site (samples 4 and 5) was nominally in the centre of each sample which in turn was opposite the phase centres of the waveguide horns. Additionally, the measurement on sample 1 was repeated several times at random sample orientations in order to judge the effects of fibre orientation with respect to the plane of polarisation and also to ascertain the experimental repeatability.

Sample 12 was secured to the frame so as to expose the measurement of permittivity at 14 sites evenly distributed across its surface plus additional sites centred at 10mm, 20mm and

40mm left and right of the designated impact site, see figure 2. A 2 Joule impact was then inflicted on the site and the permittivity measurements and ultra-sound tests repeated. The impact created a star shaped delamination with the peak extents of the delamination in the reinforcing fibre orientations and the composite surface was smoothed back into shape by hand so as to minimise the physical distortion of the sample.

IV RESULTS / DISCUSSION

A Results

The permittivity of the PTFE sample was determined to be: $\epsilon_r = 2.00 - j0.0023$ at 94GHz, which is in close agreement with previously published data ^{[7][8]}.

A summary of the ultra-sound tests and permittivity results for samples 1 to 11 is given in Table (ii). The permittivity results for sample 12 both before and after the impact is given in Table (iii). A representative sample of the ultra-sound images is given in figure 1. These are plotted on a grey-scale; pure white represents 100% transmittance whereas black indicates 0% transmittance.

B Discussion

The control samples (1, 2 and 3) of the Fibredux 916G exhibit a range in ϵ_r' of 3.76 to 3.78 and in ϵ_r'' of 0.086 to 0.099. Sample 12, also Fibredux 916G, has a spatial variation in ϵ_r' of 3.69 to 3.85 and in ϵ_r'' of 0.078 to 0.120. This composite material has reasonably consistent dielectric properties both on a sample by sample basis and within any given sample. The 3 and 2 Joule impact damages of samples 4 and 5 respectively have resulted in considerable shape distortion around the impact site and this is clearly visible on the ultra-sound images of figure 1b and 1c. This distortion has scattered the MMW signals in such a way as to yield

transmission and reflection coefficients across the measurement band which cannot be related to any value of permittivity. Clearly, the absence of a solution is resolvable from the defect-free samples. The incompletely cured samples (6, 7 and 8) differ visually in colour and feel tacky and pliable to the touch. Their ultra-sound images (figure 1d) indicate that they are ridden with defects. These samples have a variation in ϵ_r' of 3.37 to 3.61 and in ϵ_r'' of 0.074 to 0.130. The spread in ϵ_r' is outside the range of that for the nominally ideal samples (1, 2, 3 and 12) and therefore resolvable from them. The spread in ϵ_r'' is not resolvable from the nominally ideal samples. Those samples for which the vacuum was released early (9, 10 and 11) are slightly thicker than the nominally ideal samples due to the presence of large voids within them, but otherwise appear similar. Their ultra-sound images (figure 1d) indicate that they are also ridden with defects. These samples have a variation in ϵ_r' of 3.20 to 3.27 and in ϵ_r'' of 0.047 to 0.065; the reduction in both ϵ_r' and ϵ_r'' being consistent with a large material void content. The ranges of both ϵ_r' and ϵ_r'' are outside the spread in values for the nominally ideal samples and therefore are resolvable from them. Furthermore, these results are also outside the ranges for the incompletely cured samples and so are resolvable from these, too.

The ultra-sound image of sample 12, figure 1e, indicated that it had no defects. Even after the impact damage was inflicted the impact site was barely visible on the ultra-sound image, figure 1f. From a visual inspection of sample 12 a star shaped delamination was easily seen to extend 5mm left and right of the impact centre. The damage suffered by sample 12 appears to be considerably less than that of sample 5 for the same impact on the same material; indeed there is noticeably less shape distortion. No permittivity solution was found when the MMW measurement was aligned with the centre of the impact site. One may conjecture that the MMW energy is scattered from the fracture even though no foreign material is present, in the same way that light is scattered from crazed glass. However, perfectly reasonable results were obtained, which were consistent with the undamaged material, when the measurement was displaced by as little as 10mm either side of the impact centre. One might reasonably expect that the -3dB contour of the beam footprint on the

sample (circle diameter 40mm) would set the limit of spatial resolution but that large defects outside this range may still be visible to the measurement whilst minor defects within this range may not. The latter situation would appear to be the case here.

C Experimental Tolerances and Repeatability

Errors arise due to the accuracy with which the calibration is maintained, variations in sample orientation, experimental repeatability, noise modulations of the VNA results and the consistency of the sample thickness together with the accuracy to which it can be measured. However, it is not possible to anticipate what effects these error sources have on the solutions for sample permittivity due to the iterative search technique employed. The tolerance on the transmission coefficient can be significant for low-loss materials. This method is best suited to the measurement of lossy samples and has difficulty in accurately determining ϵ_r'' of low loss materials. Repeated processing of the data for extremes of all errors sources suggest a maximum variation of around $\pm 4\%$ in ϵ_r' and $\pm 25\%$ in ϵ_r'' for the composite samples. The repeated measurements on sample 12 suggest average variations in ϵ_r' of $\pm 1.0\%$ and in ϵ_r'' of $\pm 13\%$.

The fibres in the samples run in two orthogonal axes (the warp and weft of the woven samples). All the results quoted here were based on measurements conducted for the same sample orientation i.e. such that the fibres ran parallel and perpendicular to the plane of polarisation. The variability in solutions due to other random sample orientations was $< \pm 0.3\%$ in ϵ_r' and $\sim \pm 12\%$ in ϵ_r'' .

V CONCLUSIONS

The complex permittivity of PTFE and various composite samples has been determined in the 90 to 100GHz band using the free space measurement of the amplitudes of transmission and

reflection coefficient. It has then been applied to map the permittivity variation of a 500mm by 250mm sheet of 10 layer woven Fibredux 916G composite material. The variation in permittivity across the sheet was found to be $\epsilon_r' = 3.77 \pm 2.1\%$ and $\epsilon_r'' = 0.099 \pm 21\%$. This composite material has reasonably consistent dielectric properties both on a sample by sample basis and within any given sample. There are resolvable differences in the permittivity between samples of the Fibredux 916G which are nominally ideal compared with those damaged by impact, incompletely cured samples and those for which the vacuum was released during cure; each category being resolvable from the others. The measurement of the permittivity of this material can therefore be used not only as a means of detecting defects but also of determining the nature of the defect. The measurement of permittivity can find no solution for the impact damaged samples which clearly differentiates them from nominally ideal samples. The inability to find a solution is thought to arise from the shape distortion of the impact and the presence of a fracture within the material. The measurement method was successful in identifying the impact damage in sample 12, where shape distortion was minimal, even though the defect was barely visible on an ultra-sound image. The MMW technique described here is therefore more sensitive to this form of damage than the ultra-sound imaging technique. The resolution between the nominally ideal samples and those incompletely cured is based on small differences in the real part of their permittivity only. The differences are on the resolvable limit when experimental repeatability is taken into consideration. Nevertheless, an accurate measurement of permittivity has the potential to monitor the state of cure of a composite material. There are, however, clear differences in both real and imaginary parts of the permittivity between those samples in which the vacuum was released during cure and all other samples.

The spatial resolution of the measurement technique is dependent on the severity of the fault. The spatial resolution of the MMW beam on the sample was 40mm in this experiment and this should dictate the resolution of the measurement. However, the impact damaged area of sample 12 could not be resolved from the undamaged material until the equipment was aligned to within 10mm of the impact centre, suggesting a resolution of less than 10mm.

ACKNOWLEDGEMENTS

Ms Viv Wise, Cranfield University, for the manufacture of the samples.

Birmingham University, for the use of their MMW VNA facility

REFERENCES

- 1 GOPALSAMI, N., BAKHTIARI, S., DIECKMAN, S.L., RAPTIS, A.C. and LEPPER, M.J.: 'Millimeter-Wave Imaging For Nondestructive Evaluation of Materials', *Materials Evaluation*, 1994, 54, 3, pp.412-415
- 2 BAKHTIARI, S., GOPALSAMI, N. and RAPTIS, A.C.: 'Characterisation of Delamination and Disbonding in Stratified Dielectric Composites by Millimeter Wave Imaging', *Materials Evaluation*, 1995, 53, 4, pp.468-471
- 3 ALABASTER, C.M., and DAHELE, J.S.: 'Free space measurement of permittivity', *Proc. Int. Conf. on Antennas and Propagation*, April 2003, Exeter, Vol. 2, pp. 538-541
- 4 ALABASTER, C.M.: 'Permittivity of Human Skin in the Millimetre Wave Band' *IEE Electronics Letters* (accepted)
- 5 MA, Z. and OKAMURA, S.: 'Permittivity determination using amplitudes of transmission and reflection coefficients at microwave frequency', *IEEE Trans. MTT*, 1999, 47, pp. 546-550
- 6 LÄHTEENMÄKI, J and KARTTAAVI, T.: 'Measurement of dielectric parameters of wall materials at 60GHz band', *Electronics Letters*, 1996, 32, pp. 1442-4
- 7 AFSAR, M.N., TKACHOV, I.I. and KOCHARYAN, K.N.: 'A Novel W-Band Spectrometer for Dielectric Measurements', *IEEE trans. MTT*, 2000, 48, 12, pp.2637-2643
- 8 SHIMABUKURO, F.I., LAZAR, S., CHERNICK, M.R. and DYSON, H.B.: 'A Quasi-Optical Method for Measuring the Complex Permittivity of Materials', *IEEE trans. MTT*, 1984, MTT-32, 7, pp.659-665

Table and Figure captions

Table (i) Sample details

Table (ii) Samples 1 to 11 Ultra-Sound Tests & Permittivity Results

Table (iii) Sample 12 Permittivity Results

Figure 1 Ultra-Sound C-scan Images

(a) Nominally ideal (samples 1 – 3), (b) 3 Joule Impact (sample 4), (c) 2 Joule Impact (sample 5), (d) Improperly cured and early vacuum release (samples 6 – 11), (e) Large sheet (sample 12) and (f) Close up of impact zone, sample 12

White = 100% transmittance (defect-free), Black = 0% transmittance (defect)

Figure 2 Sample 12 (● = measurement centre, ✦ = impact centre. All coordinates in mm.)

Table (i)

Sample #	Defect	Composition
1, 2, 3	None – used as control	Fibredux 916G Woven 10 layers 125mm discs
4	3 Joule impact in centre	
5	2 Joule impact in centre	
6, 7, 8	Incompletely cured	
9, 10, 11	Vacuum released during cure	
12	Initially none then 2 Joule impact	500 x 250mm sheet

Table (ii)

Sample #	Ultra-sound	Permittivity
1	No defects	$3.78 - j0.086$
2	No defects	$3.78 - j0.093$
3	No defects	$3.76 - j0.099$
4	Small star shaped delamination in centre	No solution
5	Large star shaped delamination in centre	No solution
6	Defect over entire surface	$3.61 - j0.074$
7	Defect over entire surface	$3.57 - j0.130$
8	Defect over entire surface	$3.37 - j0.109$
9	Defect over entire surface	$3.20 - j0.047$
10	Defect over entire surface	$3.21 - j0.065$
11	Defect over entire surface	$3.27 - j0.053$

Table (iii)

Location (x,y in mm)	Permittivity (before damage)	Permittivity (after damage)
62.5, 62.5	3.80 – j0.115	3.90 – j0.131
85, 62.5 40mm left of impact	3.85 – j0.103	3.89 – j0.138
105, 62.5 20mm left of impact	3.85 – j0.100	3.95 – j0.127
115, 62.5 10mm left of impact	No reading	3.89 – j0.138
125, 62.5 impact site	3.84 – j0.084	No solution
135, 62.5 10mm right of impact	No reading	3.86 – j0.127
145, 62.5 20mm right of impact	3.81 – j0.088	3.86 – j0.134
165, 62.5 40mm right of impact	3.73 – j0.078	3.83 – j0.104
187.5, 62.5	3.70 – j0.120	3.73 – j0.144
250, 62.5	3.75 – j0.088	No Measurements Necessary (too remote from impact site)
312.5, 62.5	3.82 – j0.091	
375, 62.5	3.74 – j0.103	
437.5, 62.5	3.77 – 0.097	
62.5, 187.5	3.76 – j0.102	
125, 187.5	3.77 – j0.103	
187.5, 187.5	3.76 – j0.096	
250, 187.5	3.77 – j0.104	
312.5, 187.5	3.72 – j0.112	
375, 187.5	3.73 – j0.103	
437.5, 187.5	3.69 – j0.096	

Figure 1

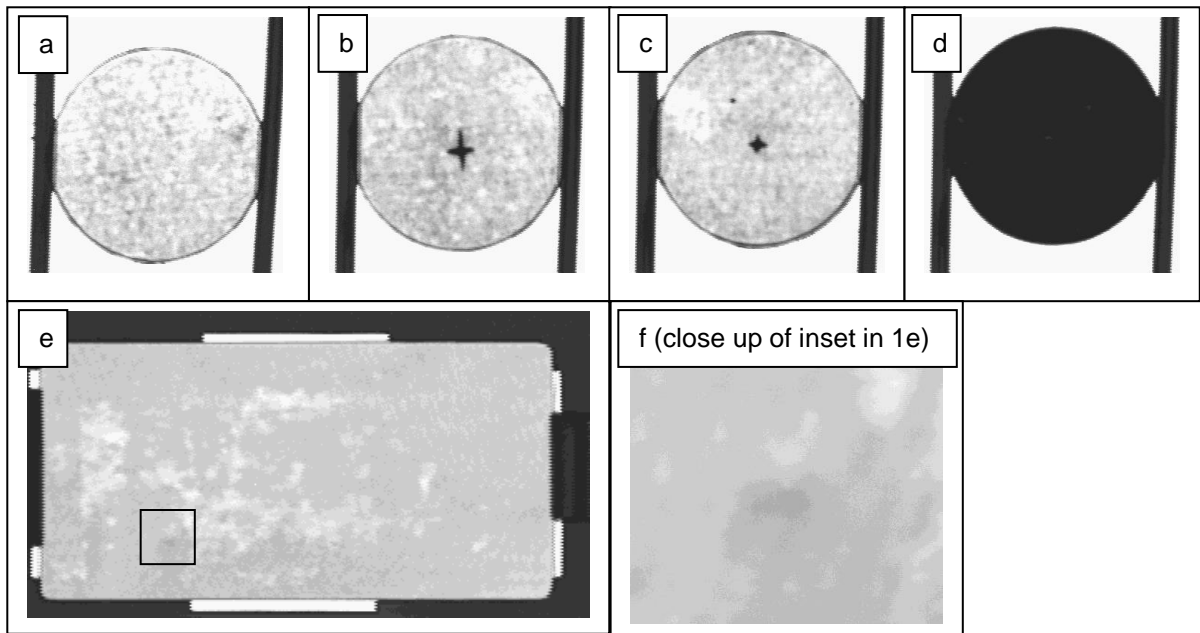


Figure 2

